Eur. J. Mineral.
2003, **15**, 649–663

Geochemical constraints on the origin of the Continental Flood Basalt magmatism in Franz Josef Land, Arctic Russia

THEODOR NTAFLOS and WOLFRAM RICHTER

Institut für Petrologie, Universität Wien – Geozentrum, Althanstr. 14, A-1090 Wien, Austria
* Corresponding author, e-mail: theodoros.ntaflos@univie.ac.at

Abstract: The Continental Flood Basalts in Franz Joseph Land, Russia, consist of basaltic andesites and tholeiitic basalts with basaltic andesites always underlying the tholeiitic basalts. Both lava types lack negative Nb-Ta anomalies precluding any interaction or assimilation of continental crust. Ratios of highly incompatible elements like Th/Ce are similar to those of the oceanic island basalts and positive ε_{Nd} values lying between MORB and Bulk Earth, indicate that the erupted magmas originated from an asthenospheric mantle plume. Major and trace element abundances that used to reconstruct the hypothetical parental magmas, indicate that for basaltic andesites this hypothetical magma originated by partial melting of an ascending plume at higher pressures than those for tholeiitic basalts.

Our model requires for basaltic andesites 11% melting of a plume at a pressure of 45 kbar. The starting picrite with 20 wt% MgO became less Mg-rich and achieved a composition of 11 wt% MgO mainly by olivine fractionation. The subsequent evolution of these lavas is characterised by fractionation processes in which clinopyroxene was the dominant phase. For tholeiitic basalts a starting picrite with 16 wt% MgO requires 23% melting of an ascending plume at a pressure of 30 kbar.

Key-words: Continental Flood Basalts, basaltic andesites, tholeiitic basalts, plumes, Arctic ocean.

Introduction

Continental Flood Basalt provinces (CFB) cover large areas with large quantities of basaltic lava flows, erupted through Precambrian (Keweenawan) to Quaternary (Snake River plain) times. As implied from the estimated duration of volcanic activity (Richards *et al.*, 1989), most of the flood basalts erupted rapidly. The viscosities of lavas were low enough to allow them to spread out as almost horizontal sheets. After sediments and MORB, CFBs are the most abundant rock type on the surface of the Earth.

CFBs are mainly tholeiitic basalts. However, basaltic andesites, dacites and rhyolites are commonly associated with such provinces. The rare occurrence of picrites is of utmost importance with respect to the petrogenesis of CFBs. The origin of flood basalts is still highly debatable and a variety of models have been developed to explain their origin.

Franz Josef Land (FJL) is an archipelago comprising over 180 (one hundred and eighty) islands, of which over 80% are covered by ice, lying east of Spitzbergen and north of Novaya Zemlya, between 44°50'- 65°20'E and 79°55'-81°51'N (Fig. 1).

Franz Josef Land consists of typical continental flood basalts. It has an aerial extension of about 70,000 km^2 and compared to other CFBs worldwide (*e.g.*, Siberian Platform, > 1.500,000 km^2) FJL is one of the smaller CFB provinces. The volume of volcanic rocks due to the lack of geophysical data, the ice cover and the post-volcanic erosion cannot be calculated. There is, however, another group of islands, the Kong Karls Land (KKL) (Fig 1.) that lies 120 km east of Spitzbergen and 400 km west of FJL which is also composed of tholeiitic basalts. These are of the same age as the FJL basalts (Parker, 1967; Kelly, 1988) and they probably belong to the same flood basalt province.

Apart from some petrographic descriptions of the FJL lavas published in Russian (Dibner & Krylova, 1963; Dibner, 1970; 1982), the rocks have been rarely studied. However, Bailey & Brooks (1988) studied five samples from Northbrook Island and one from George Land within the FJL archipelago. Their analytical results are in good agreement with ours for samples collected from the same islands. Bailey & Brooks (1988) suggested that the Franz Josef Land tholeiites formed during a Lower Cretaceous rifting stage responsible for the opening of the Canada Basin.

Although there are some preliminary reports (Ntaflos *et al.*, 1996; Ntaflos & Richter, 1998a and b; Pumhösl *et al.*, 1996), and a paper writing by Grachev (2001) presenting K-Ar dating on samples from three boreholes and geochemical-isotopic data from tholeiitic basalts, this study presents the first detailed geochemical description of the Franz Josef Land lavas. We have identified two lava series: a) tholeiitic basalts and b) basaltic andesites, and investigate their possible genetic relationships. We compared their chemical characteristics to those of other flood basalt provinces in order to

0935-1221/03/0015-0649 $ 6.75
DOI: 10.1127/0935-1221/2003/0015-0649

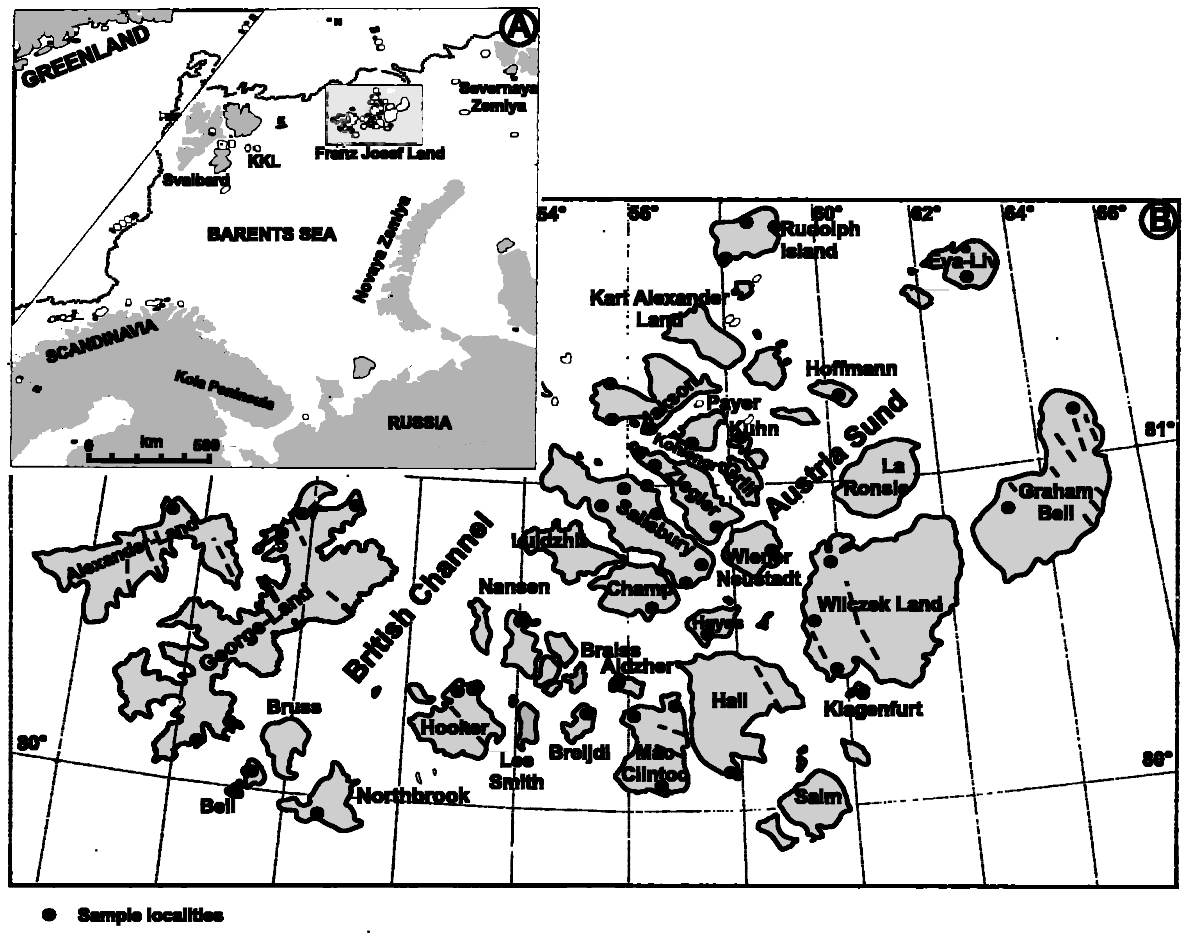

Fig. 1. (A) Overview of Barent Sea, Svalbard, Scandinavia and Novaya Zemlya. (B) Sketch map of Franz Josef Land (FJL), indicating the sample localities (black dots); dashed lines are dykes with almost SW-NE orientation.

determine similarities and/or differences that will help to shed some light on the nature of the mantle beneath Franz Josef Land.

Geological setting

The tectonic history of FJL is closely related to that of the Barents shelf. The Barents shelf is the area lying north of the Scandinavian and the western Russian Arctic mainland and west of Novaya Zemlya. It is bounded by the ocean basins of the Greenland and Norwegian Seas and by the Arctic Ocean (Kelly, 1988). FJL is situated on the northern edge of the Barents shelf (Fig 1.).

The stratigraphy of the FJL archipelago has been discussed in detail by Dibner & Krylova (1963), and Dibner (1970 and 1982), and is summarized here. The oldest rocks found in FJL are Late Triassic non-marine sediments, deposited on continental lithosphere, on the islands of Bell, Northbrook, Champ and Wilczek Land. The overlying sequences are Lower Jurassic marine sediments. The Middle Jurassic was characterized by a sandy marine transgression. Late Jurassic uplift gave rise to sandy marine deposits. Immediately after the Jurassic extensive erosion occurred. Sediments were differentially eroded resulting in a zero thickness in the west (Alexander Island), a maximum of 330 m in the central area (Wiener Neustadt and Champ Islands), and again decreasing towards the east (Wilczek Land).

The last major event recorded was the eruption of flood basalts during the Early Cretaceous. The variable thickness of the underlying sediments may have resulted from faulting due to upwelling basaltic magma followed by erosion. The lavas attain a maximum thickness of 400 m on Salisbury Island. They consist of up to five distinct lava flows with thickness varying from 3 to 90 m. Dibner (1982) and Tarakhovsky *et al.*, 1983 described sills in the eastern part of the archipelago, namely in Wilzeck Land. Doleritic dykes up to 4 m thick, with generalized NW-SW trend are abundant on the islands of Graham Bell, Hayes, George and Alexander Land (Fig. 1).

The FJL lavas are divisible into a) tholeiitic basalts and b) basaltic andesites. Lava flows of the tholeiitic basalts are sub-horizontal with columnar jointing and are frequently separated by arenaceous to argillaceous sediments up to 1 m thick. Basaltic andesites which are mainly found in the central part of the archipelago, (*e.g.*, Ziegler Island) always underlie the tholeiitic basalts and overlie the sediments. Which of these two magma series is volumetrically the dominant

one is difficult to answer because, as mentioned above, over 80% of the surface is covered by ice. Dibner (1982) reported an ultramafic intrusion of 5 km in diameter on Salisbury Island. However, despite intensive field searches in this area, the existence of this body could not be confirmed.

Age and tectonic setting

The tectonic setting of the Franz Josef Land continental flood basalts is closely related to the opening of the Arctic Ocean. Plate tectonic models based on geological and geophysical data (Jackson & Gunnarsson, 1990) suggest three stages for the evolution of the Arctic Ocean: stage I begins approximately during the Aptian (118 m.y.) creating seafloor in the Amerasia Basin. However, this reconstruction is not very accurate due to the lack of data. Stage II took place at Late Cretaceous (~80 m.y.) and Early Tertiary (~55 m.y.) and could be associated with collision of the North American and Euroasian plates. In this stage, the Lomonosov ridge is considered to have been formed as a narrow ridge of continental origin (Weber & Sweeny, 1985). Stage III, from the Early Tertiary (~55 m.y.) to the present, is associated with opening of the Eurasian Basin. The Nansen or Gakkel Ridge, which is the extension of the North Atlantic Ocean Ridge into the Arctic and divides this basin, belongs to stage III. The age of the FJL tholeiitic basalts determined by Grachev (2001) using K-Ar dating is 116 ± 5 m.y. This age is in good agreement with the $^{40}Ar/^{39}Ar$ dating age of 117 ± 2.5 m.y. determined by Pumhösl, 1998. The age of the basaltic andesites also obtained by $^{40}Ar/^{39}Ar$ is 127 ± 2 m.y. (Pumhösl, 1998).

Analytical procedures

Over three hundred and fifty samples were collected during three expeditions in the years 1993 to 1995. Care was taken to sample all stratigraphic sections from all accessible islands (Fig. 1). The samples are generally fresh without visible alteration. Olivine, however, where present, is partly pseudomorphed by serpentine. Weathered rinds and secondary veins were removed before preparation of whole-rock powders. All samples were crushed in an iron jaw crusher and subsequently reduced to powder using an agate disk mill. Major elements and the trace elements Nb, Zr, Y, Sr, Rb, Ga, Zn, Cu, Ni, Co, Sc, Cr and V were determined by XRF (Philips 2400) at the University of Vienna. Major elements were measured on fused disks and trace elements on pressed pellets. K, Na, Fe, Ni, Co, Sc, Cr, Hf, Ta, Ba, and REE were determined by INAA using the method described by Kruse & Spettel (1979). REE, Ta, and Ba in twenty samples were determined by ICP-MS (ELAN 6000).

An aliquote of 500 mg was used for Sr and Nd isotopes. Before decomposition samples were washed in warm 2.5 n HCL to remove surface contamination. Chemical sample digestion closely followed the procedure described by Thöni & Jagoutz (1992). Blank contributions are < 2 ng for Rb and Sr and < 200 pg for Nd. Rubidium, Sr, Nd and Sm concentrations were determined by isotope dilution, using mixed ^{87}Rb-^{84}Sr and ^{147}Sm-^{150}Nd spikes. Sm and Nd ID and Sr and Nd 1C samples were run as metals on a FINNIGAN MAT 262 multicollector mass spectrometer. Nd was ionized using a Re double filament. Within-run isotope fractionation was corrected for $^{146}Nd/^{144}Nd = 0.7219$ and $^{86}Sr/^{88}Sr = 0.1194$. All errors quoted are given as 2-sigma of the mean. The $^{143}Nd/^{144}Nd$ and $^{87}Sr/^{86}Sr$ ratios for the La Jolla and NBS987 international standards during the course of this investigation were 0.511847 ± 10 and 0.71023 ± 1, respectively. Errors for the $^{147}Sm/^{144}Nd$ ratio are < 1%, for the $^{87}Rb/^{86}Sr$ ratio < 2%.

Mineral compositions were measured using a CAMECA SX100 electron microprobe equipped with four wavelength-dispersive spectrometers and an EDS at the University of Vienna. Natural and synthetic minerals were used as standards.

Results and discussion

Petrographic description

Basaltic andesites are generally fresh and have glomeroporphyritic texture. Crystal clots composed of plagioclase ($An_{48}Ab_{50}Or_2$), augite ($Wo_{36}En_{41}Fs_{23}$), titanomagnetite ($Ulv_{75}Mt_{25}$), and ilmenite ($Il_{95}Ht_5$), are enclosed by fine-grained groundmass. The groundmass consists of small plagioclase laths, pyroxene, mainly pigeonite ($Wo_{10}En_{55}Fs_{35}$), titanomagnetite, ilmenite and apatite. Frequently, phenocrysts of plagioclase, and pyroxene have resorbed and embayed rims that indicate reaction with late melt. There are no compositional differences between phenocrysts and fine grained minerals.

Tholeiitic basalts have subophitic to ophitic textures with variable grain size that correspond different cooling rates. Coarse grained textures occur in the central part of a lava flow and fine grained textures occur in the bottom and in the top of the same flow. Independent of grain size, tholeiitic ba-

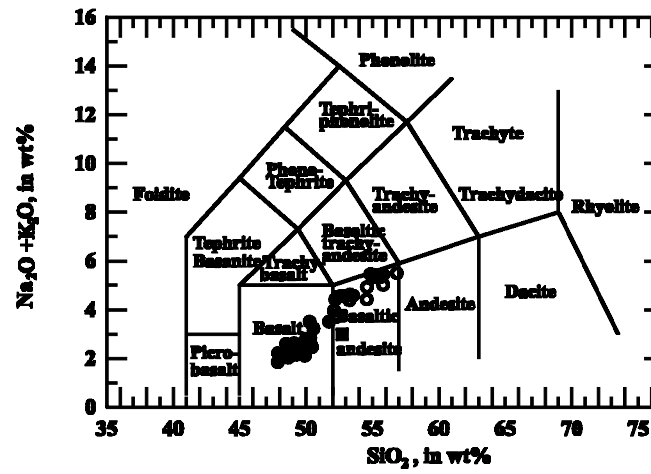

Fig. 2. Alkalies-silica plot after LeBas *et al.* (1986) for the FJL basalts; the basaltic andesites occur only in the central part of the FJL-CFB province (Fig. 1). Tholeiitic basalts: filled circles; basaltic andesites: open circles; dykes: filled square.

Table 1. Major- and trace-element analyses of Franz Josef Land samples.

Tholeiitic basalts

Sample	KU-06	MC-07	HK-03	KU-03	JK-05	GI-10	BR-03	NB-02	KU-09	MB-03	KG-02	JK-01	GI-03	GI-07	RD-02	HK-07	HK-11	NB-12	GI-02	NB-03	WZ-01
SiO_2 (wt%)	48.9	49.9	49.7	49.6	48.6	49.8	49.9	49.7	49.8	50.4	49.4	48.8	49.3	49.2	49.4	50.4	50.3	49.0	49.1	49.7	50.3
TiO_2	1.34	1.36	1.67	1.56	1.49	1.74	1.48	1.66	1.60	1.61	1.74	1.55	1.72	1.69	1.93	1.95	1.69	1.72	1.78	1.82	1.67
Al_2O_3	14.5	15.4	13.6	14.1	15.8	15.0	14.9	14.0	15.3	14.6	15.2	14.7	15.1	15.4	13.9	15.2	14.8	14.4	14.9	14.1	16.0
Fe_2O_3*	13.0	11.8	13.3	13.4	12.0	12.9	12.7	14.1	13.2	13.4	13.8	13.9	13.7	13.5	14.9	13.7	13.9	14.0	14.3	14.4	12.6
MnO	0.20	0.17	0.21	0.20	0.18	0.18	0.18	0.22	0.21	0.19	0.20	0.21	0.20	0.20	0.24	0.20	0.20	0.21	0.23	0.21	0.19
MgO	9.1	8.0	7.9	7.2	7.0	7.0	6.8	6.7	6.6	6.5	6.5	6.3	6.3	6.3	6.3	6.2	6.0	5.9	5.8	5.4	5.1
CaO	11.6	12.0	12.2	11.5	11.8	11.6	12.2	11.6	11.5	11.4	11.3	11.2	11.9	12.0	12.1	11.7	11.7	11.3	11.5	11.3	11.7
Na_2O	2.02	1.96	2.03	2.21	1.80	2.22	2.23	2.17	2.31	2.29	2.24	1.93	2.29	2.24	2.18	2.39	2.33	1.92	2.42	1.90	2.5
K_2O	0.31	0.15	0.14	0.36	0.23	0.09	0.18	0.12	0.35	0.18	0.23	0.34	0.14	0.13	0.08	0.14	0.19	0.25	0.15	0.23	0.35
P_2O_5	0.13	0.12	0.14	0.15	0.23	0.15	0.13	0.12	0.15	0.14	0.16	0.13	0.15	0.15	0.17	0.18	0.16	0.17	0.18	0.18	0.17
Total	101.03	100.84	100.96	100.28	99.11	100.58	100.66	100.42	100.94	100.63	100.67	99.00	100.71	100.81	101.13	101.91	101.28	99.01	100.35	99.20	100.60
LOI	2.17	3.1	1.24	1.91	0.41	2.37	0.94	1.84	1.80	2.41	1.30	0.51	1.29	1.83	2.02	1.62	1.77	0.93	1.46	1.39	0.63
Ba (ppm)	73	94	55	68	57	75	87	65	61	81	59	85	48	45	72	47	106	96	80	122	103
Cr	337	239	341	214	188	152	157	127	173	139	76	158	106	103	98	165	85	100	112	100	48
Ga	18	16	21	20	22	19	18	22	20	22	18	23	23	22	19	20	19	24	22	23	22
Hf	1.9	2.1	2.6	2.2	2.4	2.4	2.1	2.3	2.3	2.4	2.8	2.1	2.8	2.9	3.0	3.1	2.8	2.9	2.6	3.0	3.1
Nb	5.5	7.0	11	8.0	7.5	8.0	9.0	8.6	7.2	10	6.9	8.9	11	12	11	10	8.0	13	10	14	10
Rb	7.8	1.0	2.9	9.9	6.7	0.6	6.3	1.7	9.0	1.4	1.9	11	2.4	3.2	0.6	3.7	2.3	6.5	4.8	10	8.8
Sc	41	38	43	42	31	33	33	39	41	43	39	36	40	39	37	32	39	37	39	39	27
Sr	171	146	172	171	197	196	198	194	176	214	177	163	202	195	145	198	116	185	210	190	199
Ta	0.34	0.38	0.42	0.48	0.38	0.42	0.39	0.40	0.40	0.53	0.42	0.47	0.44	0.42	0.40	0.66	0.45	0.68	0.50	0.63	0.56
Th	0.77	0.94	0.94	1.01	0.78	0.72	1.01	1.03	0.98	1.06	0.69	0.95	0.95	0.94	0.92	1.23	1.18	1.62	0.87	1.89	1.09
U	0.18	0.20	0.25	0.29	0.19	0.20	0.23	0.00	0.28	0.27	0.13	0.22	0.21	0.21	0.35	0.40	0.33	0.38	0.22	0.39	0.30
V	274	260	350	300	267	316	301	408	303	378	359	314	375	365	374	335	361	337	354	343	269
Y	21	24	30	25	24	27	27	30	26	30	28	28	33	32	33	32	31	32	32	36	32
Zn	86	72	88	90	85	82	83	100	88	102	92	96	101	96	96	89	82	102	100	108	77
Zr	82	84	106	99	98	98	94	102	102	108	99	100	111	111	114	119	115	127	104	133	114
Co	52	47	45	48	44	38	40	45	44	44	49	43	41	46	44	39	45	43	40	42	33
Cu	139	145	169	166	151	166	149	190	160	191	182	193	179	190	198	185	195	218	186	229	195
Ni	128	98	119	91	112	78	77	73	80	68	77	85	75	77	65	79	76	73	74	71	43
La	6.5	5.5	6.5	8.3	6.6	6.4	6.8	7.4	7.9	7.2	7.0	7.0	7.5	7.6	7.5	8.6	8.5	10.0	7.4	11.0	8.3
Ce	15.9	15.4	18.4	20.9	16.7	16.5	16.8	16.5	19.4	21.2	18.4	18.5	18.1	19.3	20.3	21.4	21.3	23.4	18.8	26.5	21.1
Pr																					
Nd	10.4	10.9	13.0	12.9	12.3	0.0	12.1	12.2	12.5	13.3	12.2	12.3	13.5	14.0	14.1	14.6	13.9	13.9	14.0	18.3	14.0
Sm	3.10	3.27	3.92	3.89	3.44	3.98	3.52	3.89	3.71	3.81	3.60	3.59	4.09	4.14	4.42	4.52	4.00	4.20	3.97	4.67	4.50
Eu	1.08	1.00	1.32	1.26	1.31	1.38	1.17	1.26	1.22	1.30	1.17	1.07	1.31	1.30	1.55	1.57	1.35	1.25	1.41	1.42	1.46
Gd	0.00	0.00	0.00	0.00	0.00																
Tb	0.60	0.62	0.77	0.71	0.68		0.70	0.73	0.71	0.64	0.68	0.78	0.74	0.93	0.91	0.96	0.83	0.82	0.91	1.00	0.92
Dy																					
Ho		0.77																			
Er																					
Tm																					
Yb	2.10	2.06	2.59	2.40	2.22	3.08	2.25	2.76	2.46	2.69	2.28	2.42	2.86	3.08	3.13	2.74	2.65	2.81	2.90	3.07	2.91
Lu	0.33	0.36	0.36	0.37	0.32	0.44	0.31	0.41	0.39	0.42	0.32	0.38	0.41	0.41	0.42	0.38	0.36	0.39	0.41	0.48	0.42

*Total Fe as Fe_2O_3; blank space: not analyzed; italic numbers: ICP-MS analyses, otherwise as described in the analytical methods

Table 1. (Cont.)

Basaltic andesites

Sample	WN-02	BL-01	ZG-31	WN-03	KU-08	ZG-28	ZG-29	ZG-69	ZG-03	ZG-07	ZG-34	JK-06	JK-02	ZG-39	ZG-14	ZG-01	ZG-19
SiO_2 (wt%)	52.2	49.1	52.3	52.1	50.6	52.1	52.7	53.3	52.4	52.7	53.3	54.0	55.8	55.7	55.4	56.8	54.9
TiO_2	3.0	2.5	3.3	3.1	2.21	2.9	2.9	2.9	2.9	2.9	2.7	2.35	2.50	2.42	2.29	2.25	2.33
Al_2O_3	13.4	14.2	13.4	13.0	14.4	13.1	13.5	13.7	13.7	13.4	13.7	13.6	14.4	13.6	13.9	14.4	14.2
Fe_2O_3*	15.7	15.6	15.2	15.5	15.8	15.1	14.6	14.6	14.6	14.6	14.0	13.7	12.8	13.0	13.1	12.7	13.1
MnO	0.20	0.22	0.21	0.20	0.23	0.29	0.22	0.26	0.24	0.25	0.20	0.22	0.14	0.18	0.20	0.20	0.25
MgO	4.8	4.7	4.6	4.6	4.3	4.0	4.0	3.9	3.8	3.7	3.5	3.3	3.3	3.2	3.0	2.8	2.8
CaO	8.5	10.2	8.6	8.4	9.9	7.9	7.6	7.9	7.7	7.6	7.0	6.9	6.7	6.2	6.3	6.2	6.3
Na_2O	2.8	2.20	3.1	2.9	2.7	3.0	3.5	3.8	3.5	3.6	3.5	3.2	3.7	3.9	4.0	4.1	4.1
K_2O	0.86	0.32	0.72	0.85	0.51	1.00	1.05	0.83	1.02	0.97	1.13	1.15	1.34	1.48	1.38	1.45	1.40
P_2O_5	0.31	0.25	0.33	0.34	0.23	0.54	0.55	0.54	0.56	0.57	0.54	0.46	0.49	0.50	0.61	0.59	0.62
Total	101.80	99.32	101.63	101.03	100.82	99.86	100.64	101.66	100.29	100.27	99.53	99.06	101.12	100.16	100.22	101.54	99.97
LOI	0.76	0.89	0.24	0.82	1.63	0.08	0.52	0.39	0.29	0.26	3.3	0.45	2.7	1.05	0.24	0.21	1.12
Ba (ppm)	72	128	124	67	117	204	234	188	223	207	211	201	245	264	267	308	260
Cr	26	52	40	26	11	19	20	38	31	6	17	15	21	15	12	10	13
Ga	25	27	28	25	24	28	30	24	29	29	27	30	26	29	30	26	31
Hf	3.0	4.2	4.8	5.1	3.7	6.3		6.4	7.3	6.5	7.1	7.4	7.3	8.1		7.6	8.3
Nb	17	17	20	18	13	26	28	22	28	28	26	26	25	27	26	22	26
Rb	24	12	19	24	15	28	28	22	33	33	33	29	38	42	36	38	37
Sc	28	35	34	30	40	29	25	23	25	27	26	24	24	22	22	19	22
Sr	293	232	276	299	196	325	327	298	335	335	325	313	335	317	350	358	355
Ta	1.02	0.91	0.96	0.99	0.75	1.34	1.81	1.43	1.55	1.53	1.44	1.31	1.66	1.41	1.38	1.64	1.64
Th	1.96	1.55	1.83	2.6	1.62	2.29	3.6	3.1	4.0	2.6	3.4	3.1	4.0	4.5	3.0	4.2	4.3
U	0.46	0.35	0.36	0.57	0.38	0.42	0.93	0.80	0.93	0.76	0.89	0.84	0.81	0.94	0.85	1.12	0.93
V	389	443	403	385	358	278	257	264	280	264	229	271	278	201	183	187	189
Y	41	42	47	42	40	55	56	51	56	57	54	55	53	53	58	60	59
Zn	120	121	136	123	118	156	147	138	149	160	157	150	128	142	161	147	153
Zr	202	181	221	208	160	260	265	284	295	278	273	309	324	342	342	384	336
Co	40	39	37	41	44	28	28	25	30	25	20	30	26	24	22	21	20
Cu	121	283	56	124	287	44	47	39	58	47	39	52	67	34	20	19	23
Ni	38	51	32	39	31	18	18	11	33	18	11	22	28	16	13	14	14
La	*17.3*	12.7	15.9	19.8	12.5	24.7	*28.1*	28.1	30.8	23.4	30.1	27.2	31.8	34.9	*33.3*	37.3	36.9
Ce	*44.3*	30.5	42.1	51.1	32.1	68.3	*68.0*	65.3	73.7	54.6	71.2	67.9	79.7	74.4	*76.5*	88.1	84.9
Pr	*6.3*						*10.8*								*12.2*		
Nd	*28.5*	19.1	29.7	33.8	19.5	37.9	*43.4*	37.7	43.2	33.9	41.0	42.0	43.6	45.8	*46.9*	53.5	55.4
Sm	*6.60*	5.63	7.66	7.87	5.58	10.4	*10.6*	10.1	11.2	8.21	10.7	10.4	11.3	10.7	*11.2*	13.1	13.1
Eu	*2.46*	1.73	2.15	2.01	1.82	2.93	*3.63*	3.19	3.34	2.70	3.29	3.15	3.24	3.50	*3.70*	3.90	4.00
Gd	*6.74*						*10.78*								*11.07*		
Tb	*1.14*	1.04	1.25	1.21	1.35	1.47	*1.84*	1.90	1.76	1.31	1.68	1.64	1.73	1.67	*1.76*	2.37	1.86
Dy	*6.99*						*10.7*								*9.83*		
Ho	*1.33*						*2.32*								*2.00*		
Er	*3.21*						*5.70*								*4.93*	5.43	
Tm	*0.49*						*0.87*								*0.71*	0.81	
Yb	*2.71*	3.56	3.48	3.12	3.93	4.28	*4.91*	4.31	4.65	3.61	4.44	4.27	4.14	4.63	*4.26*	4.23	5.37
Lu	*0.35*	0.56	0.53	0.47	0.56	0.66	*0.86*	0.62	0.63	0.48	0.68	0.64	0.64	0.69	*0.63*	0.70	0.77

*Total Fe as Fe_2O_3; blank space: not analyzed; italic numbers: ICP-MS analyses, otherwise as described in the analytical methods

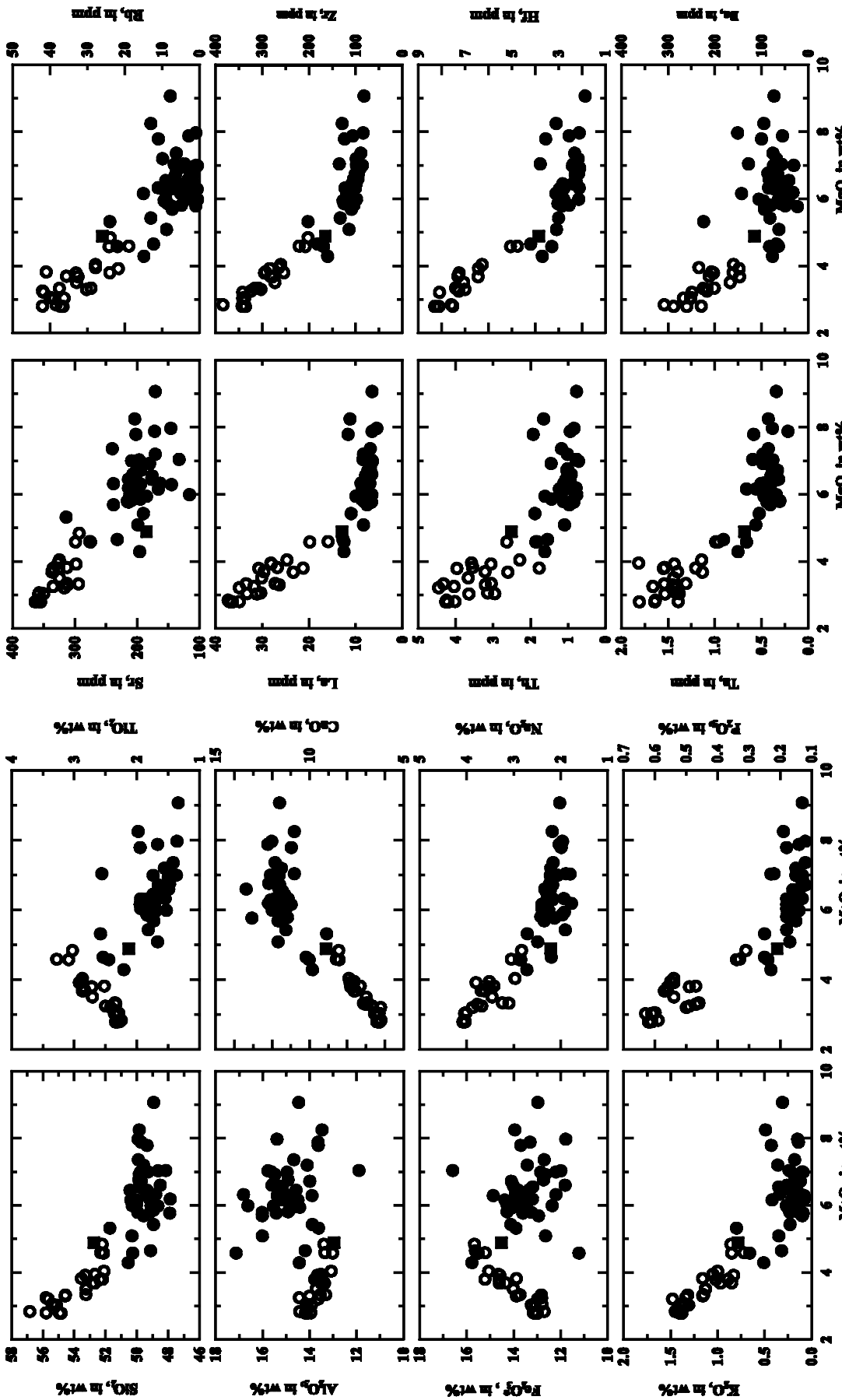

Fig. 3. Variation diagrams for FJL basalts: a) MgO *versus* major elements and b) MgO *versus* trace elements. Symbols are the same as in Fig. 2.

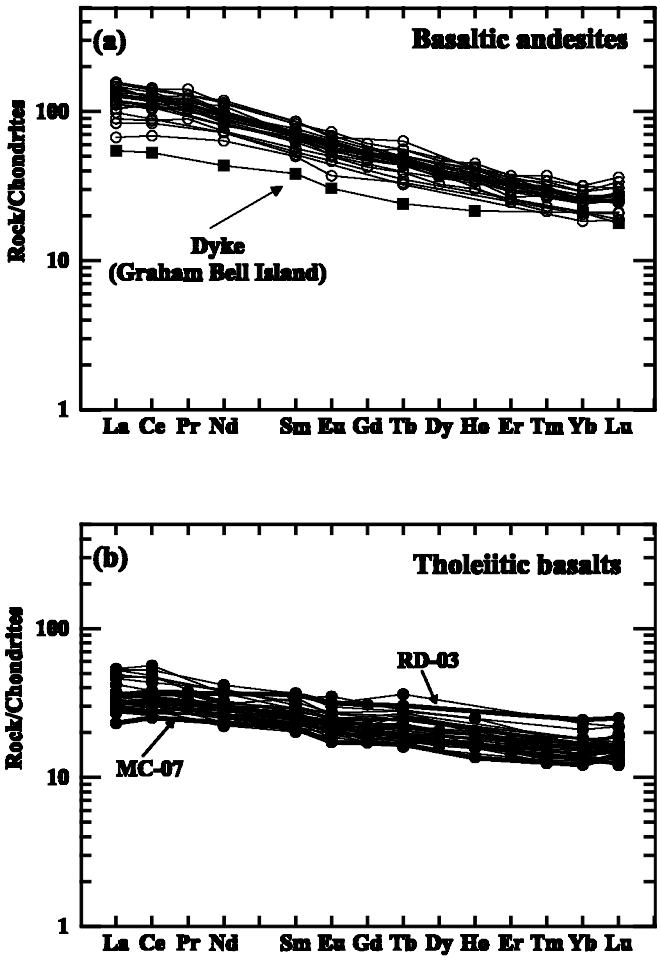

Fig. 4. Chondrite-normalized REE diagrams for (a) basaltic andesites and one dyke and (b) tholeiitic basalts. Normalizing values after Sun & McDonough (1989).

salts contain up to 2 vol% olivine, 36-45 vol% plagioclase, 33-45 vol% clinopyroxene, 5-6 vol% opaque phases (titanomagnetite and ilmenite), and variable amount, up to 11 vol%, of brownish alteration materials. Olivine grains have been, total or partial, replaced by sheet-silicates (nontronite). The Fo-content in the unaltered olivine decreases dramatically from Fo_{73} in the core to Fo_{25} in the rim. Plagioclase occurs as medium grained twinned crystals ($An_{59}Ab_{39}Or_2$) in the matrix and as coarse grained with slight oscillatory zoning phenocrysts (core, $An_{79}Ab_{20}Or_1$, and rim, $An_{60}Ab_{38}Or_2$) in clusters with augite and opaque phases. Clinopyroxene phenocrysts are Ca-rich augites with $Wo_{39}En_{47}Fs_{14}$ in the core and $Wo_{29}En_{36}Fs_{35}$ in the rim. The outermost rim consists of $Wo_8En_{31}Fs_{61}$ pigeonite. Matrix medium grained augites with $Wo_{28}En_{32}Fs_{40}$ are more Fe-rich than the phenocrysts. Opaque phases are titanomagnetites and ilmenites. Titanomagnetites vary from $Ulv_{56}Mt_{44}$ to $Ulv_{51}Mt_{49}$ with minor Al_2O_3 (0.88-1.2 wt%) and ilmenites from $Il_{98}Ht_2$ to $Il_{96}Ht_4$. They occur as large anhedral and skeletal crystals. While the titanomagnetites contain broad ilmenite exsolution lamellae, the discrete ilmenites appear to be homogeneous. Besides olivine, in samples were alteration is high, matrix augite and interstitial melt have been converted partly or totally into brownish patches consisting mainly of clay minerals.

Major and trace element geochemistry

Lavas from Franz Josef Land are divisible into tholeiitic basalts and basaltic andesites (Fig. 2) with the tholeiitic basalts overlying the basaltic andesites. Representative major and trace element analyses are given in Table 1.

a) Basaltic andesites

The MgO content in the basaltic andesites varies from 4.8 to 2.8 wt%, the TiO_2 from 3.3 to 2.25 wt% and P_2O_5 from 0.63 to 0.31 wt%. Well-defined linear trends are observed in all major and trace element variation diagrams (Fig. 3a). Negative correlations exist between MgO and SiO_2, Al_2O_3, K_2O, Na_2O and P_2O_5 whereas positive correlations are observed between MgO and CaO, Fe_2O_3 and TiO_2 (Fig. 3a).

The concentrations of the most compatible elements are low (*e.g.*, Co: 41-21 ppm, Ni: 39-11 and Cr: 40-6 ppm) but consistent with the low MgO contents suggesting homogeneous depletion after fractionation processes. The compatible elements Cr, Ni, Sc, Co and Cu, (not shown), decrease in concentration with decreasing MgO whereas Zn behaves incompatibly and shows an increase in concentration with decreasing MgO content, indicating that likely sulphide(s) phase has been removed during fractionation apparently without to affect other compatible elements. Incompatible trace element abundances (Fig. 3b) have overall trends of increasing concentrations with decreasing MgO content. Their chondrite-normalized REE patterns (Sun & McDonough, 1989), exhibit a relatively steep gradient (Fig. 4a) and the La_N/Lu_N ratio ranges from 5.7 to 3.2. The mantle-normalized incompatible element diagram (normalization factors after Sun & McDonough, 1989) displays three characteristic signatures for the basaltic andesites (1) a very distinct Sr depletion (2) a weak Ba depletion and (3) minor or not at all Nb and Ta anomalies (Fig. 5a)

b) Tholeiitic basalts

The MgO content in the tholeiitic basalts vary between 9.1 and 4.0 wt%. In contrast to the basaltic andesites the tholeiitic basalts show dispersed patterns in plots of Fe_2O_3, TiO_2, Al_2O_3, K_2O and P_2O_5 *versus* MgO (Fig. 3a). Profiles, studied on Nansen and Rudolf Islands, show that there was a general tendency for lavas to become successively less magnesian-rich up succession, suggesting progressive decrease in magma productivity (lower degrees of melting) and/or increasing degrees of fractionation with time (Table 2, Fig. 6). The alumina content, from the same profiles, however, vary more irregularly with stratigraphic height. This compositional variation among tholeiitic basalts is ascribed to variation in the mineral proportions (mainly plagioclase) in the fractionating assemblage of the individual flows. The compatible elements Cr, Ni, Sc and Co correlate positively with MgO whereas Cu (and possibly Zn) exhibits a negative correlation with MgO. The incompatible elements, compared

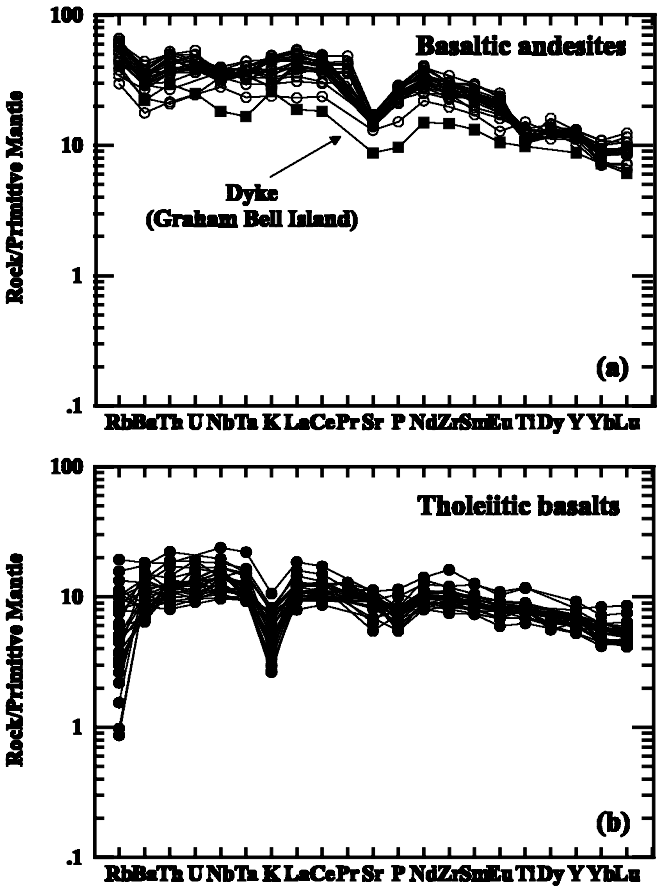

Fig. 5. Mantle-normalized incompatible elements diagrams for (a) basaltic andesites and a dyke and (b) tholeiitic basalts. Normalizing values after Sun & McDonough (1989).

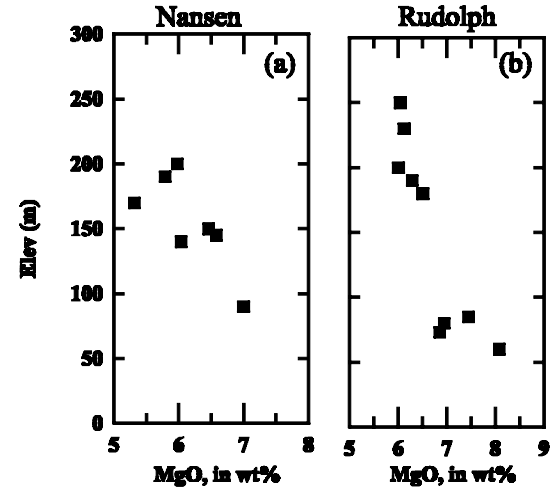

Fig. 6. Variations in MgO content of FJL lavas in selections a) from Nansen Island in the southern part of the archipelago and b) from Rudolph Island, the northermost part of archipelago. There is a general tendency for lavas to become successively less magnesian up-succession.

to those of the basaltic andesite units, are characterized by relatively low concentrations (Fig. 3b).

Chondrite-normalized REE patterns are relatively flat and their La_N/Lu_N ratios vary between 1.4 and 2.8 (Fig. 4b). The samples RD-03 and MC-07 differ from the other tholeiitic basalts because they show distinctive horizontal patterns (Fig. 4b). It is difficult to resolve their stratigraphic position and to distinguish whether these samples are sills, flows or dykes, because the largest part of the islands in the archipelago is covered permanently by ice.

Trace element abundances normalized to primitive mantle show that Ba, K, and to a lesser degree, Rb are strongly depleted relative to other incompatible elements resembling the HIMU-plume source magmas decribed by Chauvel *et al.* (1992). High Nd/P- and Zr/P-ratios indicate fractionation of garnet, or alternatively residual garnet in the source as garnet retains P during fractionation (Thompson, 1975). The low La_N/Lu_N ratios, mentioned above, that contradict the involvement of garnet in the melting processes, can be explained if garnet would be exhausted due to higher degree of partial melting. Another important feature is the absence of Nb and Ta anomalies (Fig. 5b).

Radiogenic isotopes

The Sr and Nd isotope compositions of selected tholeiitic basalts and basaltic andesites are presented in Table 3 and

Table 2. Major element concentrations of two startigraphic height profiles from Rudolf (RD) and Nansen (NA) Islands, Franz Josef Land.

Sample	RD-11	RD-12	RD-13	RD-14	RD-21	RD-20	RD-18	RD-17	RD-16	NA-1	NA-2	NA-3	NA-8	NA-4	NA-6	NA-5
Elev. in m	60	73	80	85	180	190	200	230	250	90	140	145	150	170	190	200
SiO_2	48.31	48.58	48.71	48.79	48.25	48.23	48.03	49.9	48.49	49.29	49.62	49.25	49.15	51.73	49.94	48.66
TiO_2	1.59	1.82	1.82	1.59	1.94	1.93	2.00	1.57	2.29	1.37	1.94	1.65	1.59	2.58	1.76	1.81
Al_2O_3	14.54	14.48	14.84	15.64	15.02	14.48	14.72	15.57	13.8	15.63	14.49	15.01	15.23	13.62	16.02	15.54
Fe_2O_3*	13.93	14.28	13.99	13.4	14.59	14.57	15.24	12.67	15.73	12.2	14.19	14.01	13.76	13.9	13.24	14.24
MnO	0.21	0.22	0.21	0.2	0.23	0.31	0.27	0.23	0.24	0.19	0.21	0.21	0.21	0.18	0.18	0.21
MgO	8.08	6.86	6.95	7.45	6.51	6.29	6.01	6.13	6.05	7	6.04	6.58	6.46	5.32	5.79	5.98
CaO	11.27	11.23	11.29	11.36	11.36	11.59	11.41	12.04	11.05	12.08	11.25	11.61	11.75	9.09	11.18	11.36
Na_2O	2.04	2.18	2.26	2.20	2.21	2.19	2.30	2.35	2.47	2.06	2.4	2.22	2.14	2.71	2.36	2.25
K_2O	0.23	0.26	0.26	0.23	0.16	0.13	0.11	0.17	0.14	0.1	0.21	0.16	0.15	0.8	0.23	0.14
P_2O_5	0.15	0.17	0.17	0.15	0.19	0.19	0.2	0.15	0.21	0.13	0.18	0.16	0.15	0.25	0.17	0.17
Total	100.40	100.10	100.50	101.00	100.50	99.91	100.30	100.80	100.50	100.05	100.53	100.86	100.59	100.18	100.87	100.355
LOI	0.81	0.77	0.85	0.94	0.91	0.88	0.89	0.92	1.05	0.93	1.12	0.84	0.75	1.08	1.1	0.98

*Total Fe as Fe_2O_3

Table 3. Sr and Nd isotopic analyses of Franz Josef Land samples.

Sample	$^{87}Rb/^{86}Sr$	$^{87}Sr/^{86}Sr$ measured[a]	$^{87}Sr/^{86}Sr$ initial[b]	εSr	$^{147}Sm/^{144}Nd$	$^{143}Nd/^{144}Nd$ measured[a]	$^{143}Nd/^{144}Nd$ initial[b]	εNd
Tholeiitic basalts								
KU-06	0.1319	0.70526(1)	0.70503	9.6	0.1785	0.512899(4)	0.512759	5.4
MC-07	0.0198	0.70472(1)	0.70469	4.6				
HK-03	0.0488	0.70478(1)	0.70470	4.8	0.1815	0.512867(5)	0.512724	4.7
KU-03	0.1675	0.70470(1)	0.70441	0.8	0.1817	0.512873(8)	0.512730	4.8
JK-05	0.0984	0.70418(7)	0.70401	-4.9	0.1684	0.512957(7)	0.512825	6.7
GI-10	0.0089	0.70395(1)	0.70393	-6.0				
BR-03	0.0922	0.70497(1)	0.70481	6.4				
NB-02	0.0253	0.70588(1)	0.70584	21.0	0.1920	0.512846(7)	0.512695	4.1
KU-09	0.1479	0.70470(1)	0.70445	1.2	0.1787	0.512904(6)	0.512764	5.5
MB-03	0.0188	0.70592(1)	0.70589	21.7	0.1720	0.512841(6)	0.512706	4.3
KG-02	0.0312	0.70547(6)	0.70542	15.0				
JK-01	0.1952	0.70532(1)	0.70499	8.9	0.1754	0.512852(8)	0.512714	4.5
GI-03	0.0344	0.70488(1)	0.70482	6.5	0.1826	0.512922(7)	0.512779	5.8
GI-07	0.0475	0.70481(1)	0.70473	5.2	0.1668	0.512928(7)	0.512797	6.1
RD-02	0.0124	0.70409(1)	0.70407	-4.1				
HK-07	0.0541	0.70484(1)	0.70475	5.5				
NB-12	0.1016	0.70602(1)	0.70585	21.1	0.1819	0.512781(8)	0.512638	3.0
HK-11	0.1259	0.70513(1)	0.70492	7.9	0.1819	0.512781(9)	0.512638	3.0
GI-02	0.0661	0.70494(9)	0.70483	6.6	0.1705	0.512906(6)	0.512772	5.6
NB-03	0.1523	0.70616(6)	0.70590	21.9	0.1538	0.512792(7)	0.512671	3.7
WZ-01	0.1279	0.70434(1)	0.70412	-3.4				
Basaltic andesites								
WN-02	0.2369	0.70490(1)	0.70450	1.9				
BL-01	0.1496	0.70448(1)	0.70422	-1.9	0.1775	0.512954(7)	0.512815	6.5
ZG-31	0.1991	0.70415(5)	0.70381	-7.8	0.1553	0.512967(5)	0.512845	7.1
WN-03	0.2322	0.70491(7)	0.70451	2.2				
KU-08	0.2214	0.70482(1)	0.70444	1.2	0.1724	0.512914(5)	0.512779	5.8
ZG-28	0.2474	0.70456(6)	0.70414	-3.2	0.1652	0.512925(8)	0.512795	6.1
ZG-29	0.2477	0.70406(1)	0.70364	-10.3				
ZG-69	0.2135	0.70420(1)	0.70384	-7.5				
ZG-03	0.2849	0.70443(1)	0.70394	-5.9	0.1556	0.51293(7)	0.512808	6.3
ZG-07	0.2849	0.70394(1)	0.70345	-12.9				
ZG-34	0.2937	0.70470(1)	0.70420	-2.3	0.1571	0.512909(6)	0.512786	5.9
JK-06	0.2680	0.70428(1)	0.70382	-7.6	0.1496	0.51295(7)	0.512833	6.8
JK-02	0.3281	0.70400(1)	0.70344	-13.1				
ZG-39	0.3832	0.70418(1)	0.70353	-11.8	0.1407	0.512881(6)	0.512771	5.6
ZG-14	0.2992	0.70462(1)	0.70411	-3.6				
ZG-01	0.3106	0.70413(1)	0.70360	-10.8				
ZG-19	0.3015	0.70443(1)	0.70392	-6.3	0.1425	0.512928(7)	0.512816	6.5

[a]Uncertainties reported on Sr and Nd isotope ratios are 2-sigma analytical error
[b]The age used in calculation of initial ratios and ε values is 120 m.y.
CHUR values: $^{147}Sm/^{144}Nd = 0.1967$; $^{143}Nd/^{144}Nd = 0.512638$.

summarized in Fig. 7. In the tholeiitic basalts initial $^{87}Sr/^{86}Sr$ ratios vary from 0.70405 to 0.70612 and initial $^{143}Nd/^{144}Nd$ ratios vary from 0.512651 to 0.512804 and in the basaltic andesites from 0.70375 to 0.70486 and from 0.512752 to 0.512824, respectively. With exception of four tholeiitic basalts, all other samples plot within the OIB field between the PREMA and BSE mantle components. The four tholeiitic basalts that plot outside of the OIB field have elevated $^{87}Sr/^{86}Sr$ ratios (0.70612-0.70588), probably due to hydrothermal alterations. These samples show significant devitrification of glassy residues and total or partial replacements of olivines by sheet-silicates.

Discussion

Two distinct FJL lava types

Basaltic andesites and tholeiitic basalts represent two distinct lava types. It is apparent from the variation diagrams of the major and trace elements that bulk compositional variability within both lava series is explicable in terms of fractional crystallization processes, but simple isobaric crystal fractionation from a common parent magma cannot generate the observed differences (Fig. 3a, b). The twofold distinction is best illustrated by the concentration of TiO_2 in ba-

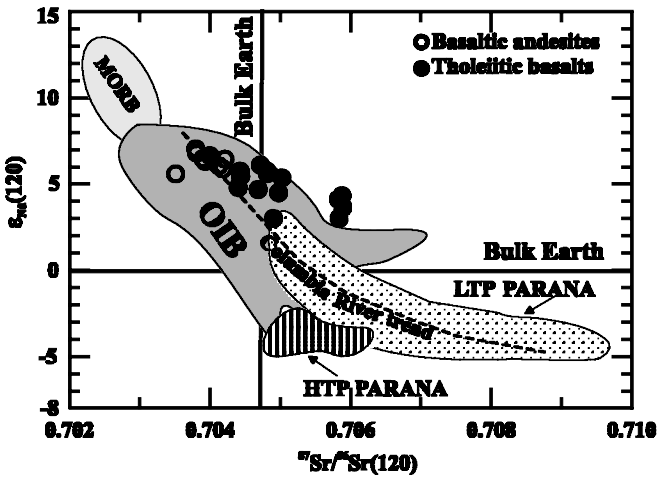

Fig. 7. Plot of initial ε_{Nd} and initial $^{87}Sr/^{86}Sr$. Most of the FJL basalts fall in the field of OIB (Zindler & Hart, 1986). Fields of Parana and Columbia River trend from Wilson (1991) and references therein.

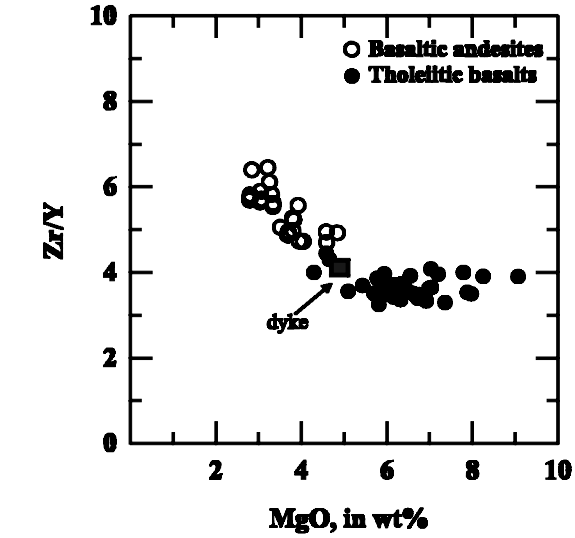

Fig. 8. Plot of MgO *versus* Zr/Y ratio for FJL basaltic andesites (open circles) and tholeiitic basalts (filled circles).

saltic andesites (high TiO_2) and tholeiitic basalts (low TiO_2). This is similar to the pattern observed for the Parana CFB province (Fodor, 1987). Furthermore, basaltic andesites have increasing TiO_2 and Fe_2O_3 with increasing MgO whereas in the tholeiitic basalts, TiO_2 and, broadly, Fe_2O_3, decrease with increasing MgO content.

Incompatible elements, when correlated with MgO, display steeper negative trends for the basaltic andesites than the tholeiitic basalts (Fig. 3b). The same correlation is illustrated by the Zr/Y vs. MgO plot in which Zr/Y ratios of tholeiitic basalts vary within narrow ranges, from 3.3 to 4.4, whereas those from basaltic andesites range from 4.7 to 6.7 (Fig. 8). Changes in slope indicate that basaltic andesites cannot be derived by fractional crystallization from the tholeiitic basalts. It is furthermore evident from the chondrite-normalized REE patterns that the basaltic andesites have overall higher REE-content than the tholeiitic basalts and that the La/Lu-ratio for the two magma types are different (Fig. 4). These steeper gradients for the basaltic andesites as

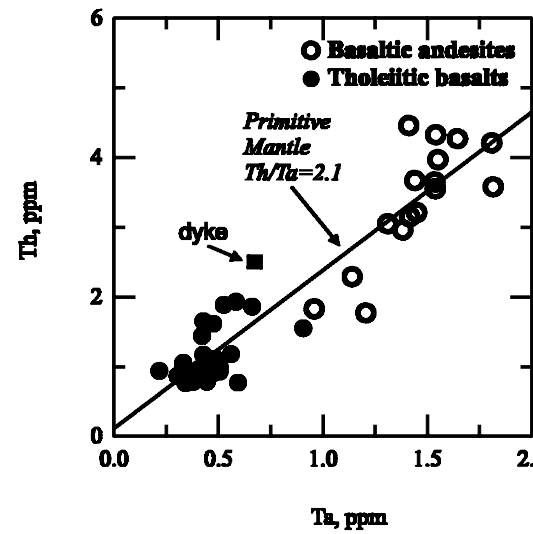

Fig. 9. Variation in Ta *versus* Th. The solid line represents the primitive mantle Th/Ta ratio (values from Sun & McDonough, 1989)

compared to tholeiitic basalts suggest that their parental magmas were derived from smaller melt-fractions than those subsequently giving rise to tholeiitic basalts. The lack of any sample with La/Nd < 1 would suggest that they were not derived from a depleted mantle source.

Crustal contamination and mantle lithosphere mixing

Negative Nb and Ta anomalies are relatively common in CFBs worldwide, and are accounted for by mixing with crustal material (Cox, 1980). An important feature of the FJL volcanism is that both lava types do not have negative Nb and Ta anomalies (Fig. 5). Another important observation is the pronounced positive correlation between Th and Ta (Fig. 9). Th/Ta ratios near 2.1 reflect eruption of both lava types with Th/Ta close to that of the primitive mantle and preclude contamination with crustal material. In addition, the tendency of both suites to have Th_N/Ta_N ratios near unity imply an asthenospheric or plume origin. Radiogenic isotopes, with exception of four, obviously hydrothermal altered tholeiitic basalts, support the asthenospheric origin because all samples plot within the OIB field (Fig. 7).

The lack of lithospheric contamination can be clearly demonstrated using ratio-ratio plots of highly incompatible elements having as denominator Ta or Nb which are essentially unaffected by fractional crystallization. Thus in the Ce/Nb *vs*. Th/Nb diagram (Fig. 10), the data from both lava series plot closely along the OIB trend indicating that both FJL lava series have originated from parental sources in which essentially no continental lithosphere was involved. However the relatively large spread of the Sr isotopes would support heterogeneous and/or distinct mantle sources. One possibility would be mixing with lithospheric component. As extensively discussed above the incompatible trace element signatures provide evidence against mixing with lithopshere. Second possible reason would be some mixing between an EM-II source and a DM source. This mixing

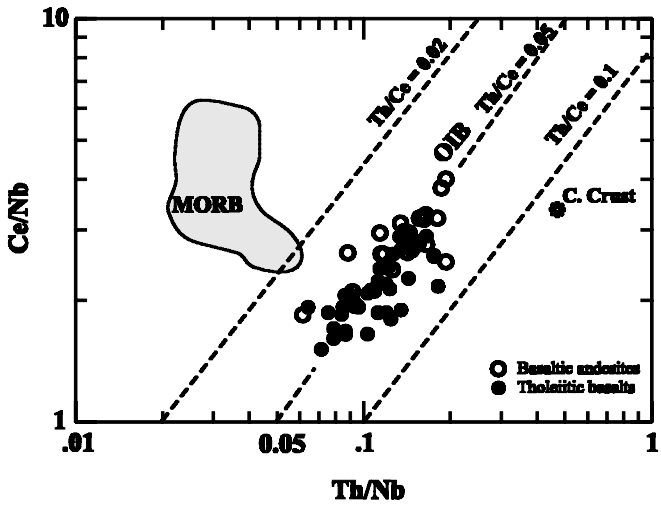

Fig. 10. Th/Nb *versus* Ce/Nb for FJL continental flood basalts. OIB Th/Ce ratio from Sun & McDonough (1989); Continental Crust from Taylor & McLennan (1985); MORB from Hofmann *et al.* (1986) and Jochum *et al.* (1983).

would explain the isotopic signature of the tholeiitic basalts. However, the EM-II components are almost exclusively restricted to the Southern Hemisphere (Zindler & Hart, 1986), and therefore this possibility can be by now rejected, unless other isotopes like Pb and Hf that are not yet available will provide evidence for the existing of an EM-II component in the Arctic region. In addition, an EM-II component would increase the Rb concentration. However, tholeiitic basalts do not show any Rb enrichment. The third possibility that could be account for the relatively large spread of the Sr isotopes may be hydrothermal alteration and/or interaction with seawater. Indeed, tholeiitic basalts that show the largest spread have subophitic textures with devitrification of glassy residues.

All the above arguments are consistent with the model advocated by Campbell & Griffiths (1990), Sharma *et al.* (1992), and Campbell (1998), in which the melting of a plume without or with minimal involvement of lithospheric mantle is the mechanism for the generation of flood basalt volcanism.

Magma sources

In order to estimate the parental magma compositions we will use petrographical observations combined with geochemical results discussed above.

Basaltic andesites

Basaltic andesites are highly evolved magmas. Therefore estimates of the parental magma composition is difficult. There are a number of arguments that support calculated estimats: (a) there is no crustal contamination (lack of negative Nb- and Ta-anomalies) (b) there is no mixing with mantle lithosphere (non-radiogenic Sr and radiogenic Nd isotopes indicate OIB signature) (c) variation diagrams exhibit linear trends that allow extrapolation of the major element abundances to more MgO-rich lavas (d) basaltic andesites are Ti-rich and have incompatible element-enriched compositions suggesting that the parental magma originated in the garnet peridotite field via relatively low degrees of partial melting. The high pressure parental picrite used in our model calculations is taken from the melting experiments on pyrolite in the range from 30 to 70 kbar as reported by Walter, 1998. This picrite has an MgO content of 20 wt% and corresponds to 11.5 % melting of a pyrolite at 1620 °C and 45 kbar (in Walter, 1998, Table 3). As olivine is the main fractionation phase at high MgO concentrations, using the olivine fractionation equation of (Pearce, 1978) we calculated that the picrites have 16, 13, and 11 wt% MgO that will be produced after fractional removing of olivine. The increase of Al_2O_3 with decreasing MgO suggests that during the evolution of the basaltic andesite lavas, not plagioclase but rather clinopyroxene was the dominant fractionation phase. In addition, the marked Sr depletion cannot be account for by plagioclase fractionation only. As Blundy & Green (2000) reported, both positive and negative Sr anomalies in melts can be generated by changes in the P-T melting conditions. For similar bulk compositions, the Sr partitioning between clinopyroxene and melt determined experimentally at 15 kbar is ~0.062 (Blundy *et al.*, 1998) and at 30 kbar ~0.128 (Hart & Dunn, 1993). Thus, Sr partitions well into clinopyroxene at high pressures, accounting for the negative Sr-anomaly relative to Ce and Nd that characterizes the basaltic andesites (Fig. 5a). Therefore, using the least-squares approximation of Bryan *et al.* (1969), removal of 6.7 % olivine, 32.5 % clinopyroxene and 10.8 % plagioclase from the picrite with originally 11 wt% MgO provides the hypothetical basalt with 6.2 wt% MgO. The evolution of the ZG-31 lava requires removal of 6.6 % olivine, 11.5 % clinopyroxene and 2.7 % plagioclase from the basalt with 6.2 wt% MgO. Final fractional removal of 21.5 % clinopyroxene, 28.4 % plagioclase and 8.0 % magnetite from lavas with ZG-31 composition provides the observed trend for basaltic andesites (Table 4, Fig 11). The mineral analyses used for modelling are given in the appendix.

Tholeiitic basalts

The most appropriate samples for modelling tholeiitic basalts are lavas from Kuhn Island in the central area of the archipelago. They have a wide range of MgO content varying from 9.1 to 4.3 wt%. The sampled lava flows have the same tendencies of decreasing MgO content with elevation as found in other islands. In addition, Sr and Nd isotopes are very similar in all lava flows from Kuhn Island, suggesting a common magma chamber.

The tholeiitic basalts, like basaltic andesites, have not experienced any crustal contamination (no negative Ta- and Nb-anomalies). Their relatively low REE contents (Fig. 4b) suggests a high degree of mantle melting. As Arndt *et al.* (1993) argue, in an ascending plume the degree of partial melting increases and the concentration of moderately to highly incompatible elements decrease. We calculated, using the method of Bryan *et al.*, 1969, the starting picrite composition for modelling the tholeiitic basalts by removal

Table 4. Compositions of model parental picrites and and their derivatives after removal of suitable amounts of ol, cpx, pl and mt.

	Basaltic andesites							Tholeiitic basalts						
ol%	12.9	8.7	5.7	6.7	3.4			3.0	5.9	2.9	5.5	6.2	6.8	
cpx%				32.5	11.5	21.5							5.4	19.0
pl%				10.8	2.7	28.4						3.4	10.1	9.5
mt%						8.0								
Sample	PBA	pic16	pic13	pic11	Bas6	ZG-31	ZG-24	PTB	pic14	pic13	pic11	KU-06	KU-03	KU-08
SiO_2	46.0	46.7	47.2	47.6	50.1	52.0	55.3	47.4	47.8	48.6	48.5	48.9	49.6	50.6
TiO_2	1.66	1.89	2.07	2.20	3.20	3.33	2.33	1.08	1.15	1.18	1.25	1.34	1.56	2.21
Al_2O_3	8.3	9.4	10.3	10.9	12.5	13.5	14.2	12.3	13.1	13.5	14.3	14.5	14.1	14.4
FeO^T	11.7	12.0	12.0	11.9	14.1	14.0	11.8	11.6	11.7	11.6	11.5	11.7	12.1	14.2
MnO	0.21	0.24	0.26	0.28	0.22	0.28	0.25	0.11	0.12	0.13	0.18	0.20	0.20	0.20
MgO	20.0	16.0	13.0	11.0	6.2	4.6	2.9	16.0	14.0	13.0	11.1	9.1	7.2	4.3
CaO	9.2	10.5	11.5	12.2	9.1	8.6	6.5	9.6	10.2	10.6	11.2	11.6	11.5	9.9
Na_2O	1.11	1.26	1.38	1.46	2.65	3.12	3.93	1.62	1.72	1.77	1.87	2.02	2.21	2.72
K_2O	0.99	1.13	1.24	1.32	0.74	0.72	1.37	0.25	0.27	0.27	0.29	0.31	0.34	0.51
Total	99.15	99.04	98.96	98.91	98.76	100.15	98.51	100.08	100.10	100.63	100.14	99.60	98.79	98.94

[T]Total Fe as FeO.

PBA = parental picrite for basaltic andesites derived by 11 % partial melting of a gt-peridotite at 45 kbar (see appendix).

The column above each liquid represents the mineral proportions removed in order to form the next liquid with lower MgO content (*e.g.* pic16 formed by 12.9 % olivine fractional removal of PBA).

PTB = parental picrite for tholeiitic basalts derived by partial melting of a gt-peridotite at 30 kbar (see appendix).

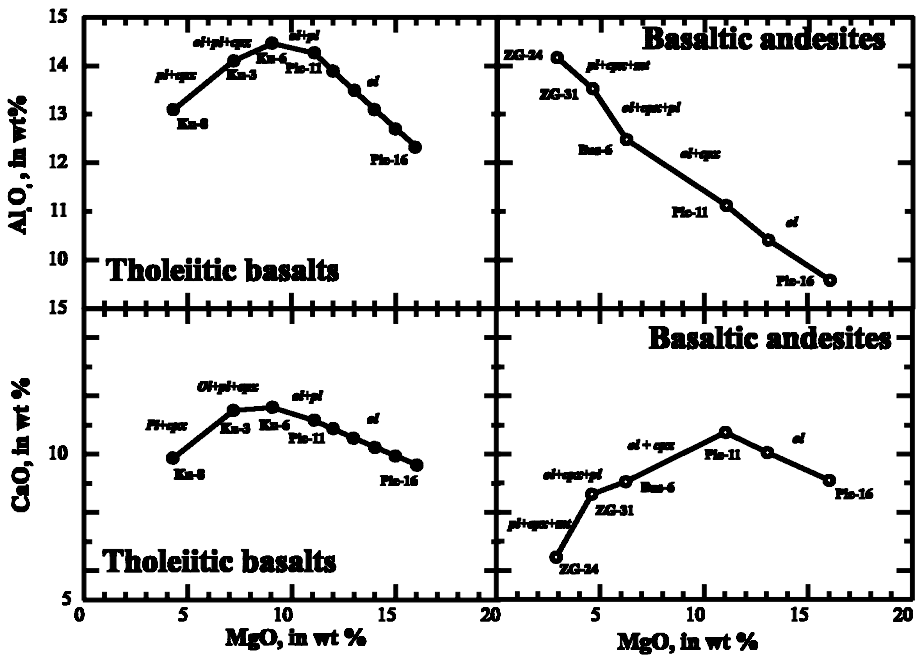

Fig. 11. MgO *versus* CaO and Al_2O_3 variation diagrams for the calculated lavas.

of 55.7 % olivine, 10.13 % orthopyroxene, 4.4 % clinopyroxene and 6.3 % garnet of a pyrolitic mantle composition (McDonough & Sun, 1995). This corresponds to 23.3 % melting of a primitive mantle. The mineral compositions used in this model are from Matsoku garnet lherzolites equilibrated at 30 kbar (Cox *et al*., 1973). Using the same procedure as for the modelling of the basaltic andesites, we calculated the mineral phase proportions that should be removed in order to model the trends observed for major elements (Fig. 11).

Our model, without to claim that it represents the only explanation to the evolution of the FJL flood basalts, is consistent with the model proposed by Arndt *et al.* (1993). In this model Arndt *et al.* (1993) argued that melt of low-degree melting (high-Ti flood basalts) can be formed at high pressures beneath a thick lithosphere and melts of high-degree melting (low-Ti basalts) can be formed at lower pressures beneath a thinner lithosphere. Fodor (1987), without to consider the possible effect of lithospheric thickness, suggested differences in the degree of partial melting of the same magma source as the reason for the existence of high- and low-Ti flood basalts in Parana. The geographic correlation between both lava types, the high-Ti lavas occur in the northern part and the low-Ti lavas in the southern part, led Fodor (1987),

to suggest that they represent partial melting of different parts of a mantle plume. Hawkesworth *et al.* (2000) suggested that the high- and low-Ti lavas of the Parana-Etendeka province have been derived from the lithospheric mantle by different melt generation rates as a consequence of different amount of extension. The FJB high- and low-Ti lavas, to our knowledge, do not show any geographical correlation. The tholeiitic basalts (low-Ti lavas) overlay the basaltic andesites (high-Ti lavas) and therefore the model of sampling the same plume at different places as suggested by Fodor, 1987, cannot be applied for. On the other hand their geochemical evidence clearly suggests that FJL Flood basalts have been derived from asthenospheric and not from lithospheric mantle.

The Arctic large(?) igneous province

The direct relation of the Franz Josef Land volcanism to the Lomonosov or to Nansen Ridge is not obvious as the age of the tholeiitic basalts determined by Grachev (2001) using K-Ar dating is 116 ± 5 m.y. which is in good agreement with the $^{40}Ar/^{39}Ar$ dating age of 117 ± 2.5 m.y. determined by Pumhösl, 1998. The age of the basaltic andesites obtained also by $^{40}Ar/^{39}Ar$ is 127 ± 2 m.y. (Pumhösl, 1998). Thus, the Franz Josef Land basalts are clearly older than the Lomonosov and Nansen Ridges and cannot be related.

In the Arctic Region a number of localities exhibit similar magmatism. The Kong Karls Land basalt flows (Fig. 1) with similar geochemical characteristics, like absence of Nb and Ta anomalies and a Th/Ta ratio of *ca*. 2.1 (Ntaflos & Richter, 1998b), have an age between 120 and 110 m.y. (Smith *et al.*, 1976) and it is broadly consistent with the age of the Franz Josef Land basalts. Also the flood basalts of the Axel Heiberg Island in the Canadian Arctic show similarities to the Franz Josef Land in terms of age and geochemistry (Thorsteinsson & Tozer, 1970).

The appearance of flood basalt volcanism of broadly the same age and scattered all over the Arctic region may be part of a large igneous province associated with major tectonic formations (*e.g*., Alpha Ridge) that are related to the Arctic continental breakup. The source of this large igneous province could be considered an ascending plume. The geochemical data, presented above, verify the plume origin of the Franz Josef Land flood basalts and as they do not show any interaction with lithosphere (mantle and crust) the plume-head hypothesis mechanism developed by Cambell & Griffiths, 1990 could be considered as the source of the large Arctic igneous province. The *ca*. 10 m.y. age gap between basaltic andesite and tholeiitic basalt eruptions can be explained within the frame of the plume-head hypothesis in which the main phase of volcanism is followed by a period of extension and lithospheric thinning (the opening of the Arctic ocean basin) that may lead to a second phase of volcanic activity (Campbell, 1998).

Conclusions

The Continental Flood Basalt province of Franz Joseph Land, compared to the other world-wide provinces of this type, is a relatively small one. Both, basaltic andesites and tholeiitic basalts have geochemical and isotopic characteristics of asthenospheric origin. The elemental ratios of highly incompatible elements like Th/Ce have values similar to those of the oceanic island basalts. The isotopic compositions are similar to those of the postulated asthenospheric mantle source. The Th/Ta ratios of approximately 2.1 in both lava types indicate that magma source(s) preserved their primitive mantle compositional trend. In addition, the absence of negative Nb and Ta anomalies show that crustal assimilation was not a significant process during the evolution of the FJL CFBasalts. Thus, the dominant source of both lava types was likely an ascending mantle plume.

Our model calculations show that the source for the basaltic andesites experienced about 11 % patial melting of a plume at a depth of ca. 140 km and for the tholeiitic basalts 23 % partial melting of the same source at shallower depth (*ca.* 100 km).

Acknowledgments: We wish to thank Misha Nazarov for providing translations of various Russian publications and K. Petrakakis and P. Nagl for XRF-analyses and M. Thöni and A. W. Hofmann for the isotopic analyses. The Federal Ministery for Education, Science and Culture and the FWF (P.I. W. Richter) provided financial support. Thanks to Wolgang Siebel, Torse Vennemann, and an anonymous reviewer for thorough and constructive reviews of the original manuscript. Also we would like to thank Gero Kurat, Igor Ryabchikov and Brain Upton for critical reading of a previous version of this paper.

References

Arndt, N.T., Czamanske, G.K., Wooden, J.L., Fedorenko, V.A. (1993): Mantle and crustal contributions to continental flood volcanism. *Tectonophysics*, **223**, 39-52.

Bailey, J.C. & Brooks, C.K. (1988): Petrochemistry and tectonic setting of Lower Cretaceous tholeiites from Franz Josef Land, U.S.S.R. *Geol. Soc. Denmark*, **37**, 31-49.

Blundy, J.D. & Green, T. (2000): A partitioning origin for Strontium anomalies in mantle-derived melts. *J. Conf. Abstr.*, **5**(2), 219.

Blundy, J.D., Robinson, J.A.C., Wood, B.J. (1998): Heavy REE are compatible in clinopyroxene on the spinel lherzolite solidus. *Earth Planet. Sci. Lett.*, **160**, 493-504.

Bryan, W.B., Finger, L.W., Chayes, F. (1969): Estimating proportions in petrographic mixing equations by least-squares approximation. *Science*, **163**, 926-927.

Campbell, I.H. (1998): The mantle's chemical structure: Insights from the melting products of mantle plumes. *in* "The Earth's Mantle: composition, structure, and evolution", Jackson, I., ed., Cambridge University Press, Cambridge, 259-310.

Campbell, I.H. & Griffiths, R.W. (1990): Implications of mantle plume structure for the evolution of flood basalts. *Earth Planet. Sci. Lett.*, **99**, 79-93.

Chauvel, C., Hofmann, A.W., Vidal, P. (1992): HIMU-EM: The French Polynesian connection. *Earth Planet. Sci. Lett.*, **110**, 99-119.

Cox, K.G. (1980): A model for flood basalt volcanism. *J. Petrol.*, **21**, 629-650.

Cox, K.J., Gurney, J.J., Harte, B. (1973): Xenoliths from the Matso-

ku pipe. *in* "Lesotho Kimberlites", Nixon, P.H., ed., Lesotho Nat. Devel. Corp., 76-91.

Dibner, V.D. (1970): Franz Josef Land and Victoria Island. *in* "Geologiya SSSR", Sidorenko, A.V., ed., Nedra, Moscow, 60-108 (in Russian).

– (ed.) (1982): Microfossils of the polar regions and their importance. *PGO 'Sevmorgeologiya'*, Leningrad, 114 pp. (in Russian).

Dibner, V.D. & Krylova, N.M. (1963): Stratigraphic position and material composition of coal measures in Franz Josef Land. *Int. Geol. Rev.*, **7**, 1030-1038.

Fodor, R.V. (1987): Low- and high-TiO_2 flood basalt of southern Brazil: origin from picritic parentage and a common mantle source. *Earth Planet. Sci. Lett.*, **84**, 423-430.

Grachev, A.F. (2001): A new view on the origin of magmatism of the Franz Josef Land. *Izvestyia, Physics of the Solid Earth*, **37**, 744-756.

Hart, S.R. & Dunn, T. (1993): Experimental cpx/melt partitioning of 24 trace elements. *Contrib. Mineral. Petrol.*, **113**, 1-8.

Hofmann, A.W., Jochum, K.P., Seufert, M., White, W.M. (1986): Nb and Pb in oceanic basalts: new constraints on mantle evolution. *Earth Planet. Sci. Lett.*, **79**, 33-45.

Jackson, H.R. & Gunnarsson, K. (1990): Reconstruction of the Arctic; Mesozoic to present. *Tectonophysics*, **172**, 303-322.

Jochum, K.P., Hofmann, A.W., Ito, E., Seufert, H.M., White, W.M. (1983): K, U, and Th in mid-ocean ridge basalt glasses and heat production, K/U and K/Rb in the mantle. *Nature*, **306**, 431-436.

Kelly, S.R.A. (1988): Jurassic through Cretaceous Stratigraphy of the Barents Shelf. *in* "Geological Evolution of the Barent Shelf Region", Harland, W.B. & Dowdeswell, E.K., eds., Graham and Trotman, London, 109-130.

Kruse, H. & Spettel, B. (1979): A combined set of automatic and interactive programs for instrumental neutron activation analysis. *J. Radioan. Chem.*, **70**, 427-434.

LeBas, M.J., LeMaitre, R.W., Streckeisen, A., Zanettin, B. (1986): A chemical classification of volcanic rocks based on the total alkali silica diagram. *J. Petrol.*, **27**, 745-750.

McDonough, W.F. & Sun, S.-s. (1995): The composition of the Earth. *Chemical Geol.*, **120**, 223-253.

Ntaflos, Th. & Richter, W. (1998a): Continental Flood Basalts from Franz Josef Land, Arctic Russia. Evidence for bimodal magmatism. III Int. Conf. on Arctic Margins, 131-132.

–, – (1998b): Sind die Plateaubasalte des Franz Josef Landes und des Kong Karls Landes Teile einer grösseren gemeinsamen Eruptivprovinz? *Mitt. Österr. Min. Ges.*, **143**, 355-336.

Ntaflos, Th., Richter, W., Thöni, M., Hofmann. A., Pumhösl, H. (1996): The Early Cretaceous Continental Flood Basalts from Franz Josef Land, Arctic Russia. *J. Conf. Abstr.*, **1**, 438.

Parker, J.R. (1967): The Jurassic and Cretaceous Sequence in Spitsbergen. *Geol. Mag.*, **105**, 87-505.

Pearce, T.H. (1978): Olivine fractionation equation for basaltic and ultrabasic liquids. Nature, **276**, 771-774.

Pumhösl, H. (1998): Petrographische und geochemische Untersuchungen an den Deckenbasalten der Insel Salisbury, Franz Joseph-Land, russische Arktis. University of Vienna, Master thesis, 120 p.

Pumhösl, H., Ntaflos, Th., Richter, W. (1996): Kontinentale Deckenbasalte von Franz Joseph Land am Beispiel der Insel Salisbury. *Österr. Min. Ges.*, **141**, 182-183.

Richards, M.A., Duncan, R.A., Courtillot, V. (1989): Flood Basalts and Hot-Spot Tracks: Plume Heads and Tails. *Science*, **246**, 103-107.

Sharma, M., Basu, R.A., Nesterenko, G.V. (1992): Temporal Sr-, Nd- and Pb-isotopic variations in the Siberian flood basalts: Implications for the plume-source characteristics. *Earth Planet. Sci. Lett.*, **113**, 365-381.

Smith, D.G., Harland, W.B., Hughes, N.F., Pickton, C.A.G. (1976): The geology of Kong Karls Land, Svalbard. *Geol. Mag.*, **113**, 193-232.

Sun, S.-s. & McDonough, W.F. (1989): Chemical and isotopic systematics of oceanic basalts: implications for mantle composition and processes. *in* "Magmatism in the Ocean Basin", Saunders, A.D. & Norry, M.J., eds., *Geol. Soc. Spec. Publ.*, **42**, 313-345.

Taylor, S.R. & McLennan, S.M. (1985): The Continental Crust: Its Composition and Evolution. Oxford, Blackwell, 312 p.

Tarakhovsky, A.N., Fischman, M.V., Shkola, I.V., Andreichev, V.L. (1983): Age of Franz Josef Land Traps. *Dokl. Akad. Nauk. SSSR*, **233**, 965-969.

Thompson, R.N. (1975): Is upper-mantle phosphorus contained in sodic garnet? *Earth Planet. Sci. Lett.*, **26**, 417-424.

Thorsteinsson, R. & Tozer, E.T. (1970): Geology of the Arctic Archipelago. *in* "Geology and Economic Minerals of Canada", Douglas, R.J.W., ed., Geological Survey Canada, 547-590.

Thöni, M. & Jagoutz, E. (1992): Some new aspects of dating eclogites in orogenic belts: Sm-Nd, Rb-Sr, and Pb-Pb isotopic results from the Austroalpine Saualpe and Koralpe type-locality (Carinthia/Styria, southeastern Austria). *Geochim. Cosmochim. Acta*, **56**, 347-358.

Walter, M.J. (1998): Melting of garnet peridotite and the origin of komatiite and depleted lithosphere. *J. Petrol.*, **39**, 29-60.

Weber, J.R. & Sweeny, J.F. (1985): Reinterpretation and crustal structure in the central Arctic Oceanic basin. *J. Geophys. Res.*, **90**, 663-677.

Wilson, M. (1991): Igenous Petrogenesis; a global tectonic approach. Harper Collins Academic, London, 466 p.

Zindler, A. & Hart, S. (1986): Chemical geodynamics. *Earth Planet. Sci. Lett.*, **14**, 493-571.

Received 2 July 2002
Modified version received 10 January 2003
Accepted 26 March 2003

Appendix

Table A. Model parental liquids for basaltic andesites and tholeiitic basalts formed by melting of pyrolitic mantle composition.

		Basaltic andesites				Tholeiitic basalts				
	1	2	3	4	5	6	7	8	9	10
Sample	McDS	ol	cpx	gt	PBA	PTB	ol	opx	cpx	gt
SiO_2	45.00	40.10	55.14	42.70	46.00	47.42	40.63	57.60	55.90	41.80
TiO_2	0.20		0.10	0.40	1.70	1.08	0.03	0.04	0.08	0.09
Al_2O_3	4.45	0.20	3.51	22.54	8.30	12.34		0.75	2.23	21.62
FeO*	8.05	9.10	5.00	5.50	11.73	11.63	7.50	4.60	2.56	7.40
MnO	0.14	0.13	0.13	0.19	0.21	0.11	0.09	0.09	0.08	0.36
MgO	37.81	49.71	26.80	23.45	20.07	16.00	50.32	35.02	17.12	20.82
CaO	3.55	0.30	7.53	4.30	9.20	9.64	0.04	0.56	19.71	5.12
Na_2O	0.36		0.70		1.10	1.63		0.13	2.18	
K_2O	0.03				1.00	0.26				
Total	99.59	99.54	98.91	99.08	99.31	100.11	98.61	98.79	99.86	97.21
Proportions of minerals being melted		52.54	24.35	11.07	12.06[a]	23.32[a]	55.86	10.13	4.40	6.31

Notes:
McDS: pyrolitic model mantle composition of McDonough & Sun (1995); 2, 3, 4: mineral compositions used for calculations at 45 kbar after Walter (1998); PBA: parental picrite for basaltic andesites; PTB: parental picrite for tholeiitic basalts; 7, 8, 9, 10: mineral compositions used for calculations at 30 kbar after Cox *et al.* (1973);
[a] liquid formed after partial melting of the McDS.
* Total Fe as FeO.

Table B. Mineral compositions used for calculations of the basaltic andesites in Table 4.

	ol		cpx			pl		mt
Sample	pic11	Bas6	pic11	Bas6	ZG-31	Bas6	ZG-31	ZG-31
SiO_2	40.0	37.2	50.1	49.8	51.4	53.3	61.6	0.30
TiO_2	<0.02	<0.02	2.09	1.34	0.95	0.01	0.10	18.8
Al_2O_3	<0.02	0.00	2.42	3.7	1.43	28.4	24.5	2.20
FeO*	14.5	29.3	7.5	11.3	13.5	0.80	0.80	68.9
MnO	0.18	0.40	0.13	0.27	0.38	0.04	0.04	0.48
MgO	45.5	33.5	16.3	15.6	14.9	0.12	0.04	3.1
CaO	<0.02	0.04	20.7	17.6	17.6	12.4	6.9	<0.02
Na_2O	<0.02	<0.02	0.31	0.36	0.30	4.42	6.9	<0.02
K_2O	<0.02	<0.02	<0.02	<0.02	<0.02	0.15	0.66	<0.02
Total	100.20	100.42	99.48	99.95	100.34	99.64	101.59	93.79

Table C. Mineral compositions used for calculations of the tholeiitic basalts in Table 4.

	ol		cpx		pl		
Sample	pic11	KU-06	KU-06	KU-03	pic11	KU-06	KU-03
SiO_2	40.0	37.8	51.6	51.7	47.7	49.3	51.4
TiO_2	<0.02	0.02	0.70	0.70	0.03	0.04	0.05
Al_2O_3	<0.02	0.03	2.00	2.46	33.3	31.1	31.3
FeO*	14.2	25.1	10.4	9.0	1.04	0.74	0.83
MnO	0.13	0.18	0.11	0.10	0.02	0.02	0.02
MgO	45.8	37.2	16.1	16.3	0.04	0.13	0.10
CaO	<0.02	0.32	18.7	19.6	17.3	15.1	14.5
Na_2O	<0.02	0.05	0.20	0.20	1.54	2.9	3.5
K_2O	<0.02	<0.02	<0.02	<0.02	0.08	0.09	0.10
Total	100.08	100.68	99.80	100.04	101.04	99.43	101.80

* Total Fe as FeO.